

# Calcination Atmosphere Regulated Morphology and Catalytic Performance of Pt/SiO<sub>2</sub> in Gas-phase Oxidative Dehydrogenation of KA-oil

Wei Hong<sup>+</sup>,<sup>[a]</sup> Zhi-Qiang Wang<sup>+</sup>,<sup>[b]</sup> Shihui Zou,<sup>\*,[a]</sup> Yuheng Zhou,<sup>[a]</sup> Linfang Lu,<sup>[a]</sup> Qiuyue Zhou,<sup>[a]</sup> Xue-Qing Gong,<sup>\*,[b]</sup> and Jie Fan<sup>\*,[a]</sup>

It is industrially attractive to produce cyclohexanone directly from gas-phase oxidative dehydrogenation (ODH) of KA-oil (a mixture of cyclohexanone and cyclohexanol) since extra alcohol-ketone separation process can be potentially omitted. Herein, by simply tuning the calcination atmosphere of Pt/SiO<sub>2</sub>, we successfully regulated the morphology of Pt nanoparticles and optimized their catalytic performance in ODH of KA-oil. Pt/

SiO<sub>2</sub> calcined in O<sub>2</sub> atmosphere showed a cube-like morphology and achieved a 78.1% cyclohexanone yield at 170 °C, which surpassed its counterpart calcined in H<sub>2</sub> and most of the reported catalysts. Further experimental and theoretical calculation results indicated that cubic Pt nanoparticles possessed stronger adsorption ability to cyclohexanol and therefore performed better in ODH of KA-oil.

## Introduction

Cyclohexanone is a very important and versatile intermediate in current chemical industrial practices as it is frequently used in the production of  $\epsilon$ -caprolactam for the manufacture of nylon-6.<sup>[1]</sup> Industrially, cyclohexanone is mainly produced in the form of KA-oil (a mixture of cyclohexanone and cyclohexanol) by selective oxidation of cyclohexane.<sup>[2]</sup> Due to the close boiling points of cyclohexanone and cyclohexanol (155 °C vs. 161 °C), an energy-intensive distillation separation is generally required to produce pure cyclohexanone.<sup>[3]</sup> For the purpose of simplifying operations and saving energy, it is highly attractive to develop gas-phase oxidative dehydrogenation (ODH) of KA-oil that can potentially achieve a 100% yield of cyclohexanone. However, the reported catalytic systems are still far from affording a cyclohexanone yield (~100%) that is able to omit the alcohol-ketone separation process. Typically, the reported conversion in ODH of cyclohexanol is less than 80% and a high reaction temperature is generally required (typically 230–340 °C, see Table 1 below). When KA-oil is used as the substrate, the competitive adsorption between cyclohexanol and cyclohexa-

none further decreases the activity (entry 6 and 9 in Table 1). To this end, developing advanced catalysts that can strengthen the adsorption of cyclohexanol and weaken the adsorption of cyclohexanone has become a focus in this area.

It has long been recognized that the morphology (exposed crystal planes) of the active nanoparticles is an important factor affecting the adsorption ability and catalytic performance of the catalyst.<sup>[4]</sup> For instance, Lee *et al.* found that the isomerization of *trans*-2-butene to *cis*-2-butene was promoted by Pt(111) faces due to the extra stability of *cis*-2-butene on hydrogen-saturated Pt(111) surfaces.<sup>[4c]</sup> Considering Pt was recently reported as an efficient catalyst for selective oxidation of KA-oil,<sup>[5]</sup> we reasoned that a precise control over the morphology might be able to optimize the adsorption of cyclohexanol/cyclohexanone and therefore further improve the catalytic performance of Pt in ODH of KA-oil.

Unlike the sophisticated colloid synthesis,<sup>[6]</sup> in this work, the morphology of Pt nanoparticles (PtNPs) was tuned simply by a calcination of Pt/SiO<sub>2</sub> in different atmospheres. The absence of ligand modification provided a clean surface to investigate the correlation between Pt facets and activity. The cube-like PtNPs obtained by calcinating Pt/SiO<sub>2</sub> in O<sub>2</sub> (denoted as Pt/SiO<sub>2</sub>-O) exhibited a much better catalytic performance in ODH of KA-oil than round-edged PtNPs, which were produced by calcinating Pt/SiO<sub>2</sub> in H<sub>2</sub> (denoted as Pt/SiO<sub>2</sub>-H). Pt/SiO<sub>2</sub>-O presented a yield of cyclohexanone as high as 78.1% at 170 °C, exceeding most of the reported catalysts (Table 1). Combining the extensive kinetic data with theoretical calculations, we successfully revealed the relationship between the morphology of PtNPs and the adsorption ability and catalytic performance of PtNPs.

## Results and Discussion

Shape-controlled synthesis of metal nanocatalysts is a very hot topic in the catalysis research. In addition to the classic colloid

[a] W. Hong,<sup>+</sup> Dr. S. Zou, Y. Zhou, Dr. L. Lu, Q. Zhou, Prof. J. Fan  
Key Lab of Applied Chemistry of Zhejiang Province  
Department of Chemistry  
Zhejiang University  
Hangzhou 310027, (P.R. China)  
E-mail: jfan@zju.edu.cn  
xueshan199@163.com

[b] Z.-Q. Wang,<sup>+</sup> Prof. X.-Q. Gong  
Key Laboratory for Advanced Materials  
Centre for Computational Chemistry and Research Institute of Industrial Catalysis  
East China University of Science and Technology  
Shanghai, 200237, (P.R. China)  
E-mail: xgong@ecust.edu.cn

[<sup>+</sup>] These authors contributed equally to this work.

 Supporting information for this article is available on the WWW under <https://doi.org/10.1002/cctc.201801279>

**Table 1.** Gas-phase oxidative dehydrogenation of cyclohexanol or KA-oil to cyclohexanone.<sup>[a]</sup>

| Entry             | Catalyst               | Substrate    | Oxidant                                 | Temperature [°C] | Cyclohexanol conversion [%] | Cyclohexanone yield [%] | Reference |
|-------------------|------------------------|--------------|---|------------------|-----------------------------|-------------------------|-----------|
| 1                 | ETS-10                 | cyclohexanol | Air                                     | 250              | 49.7                        | 33.6                    | [1c]      |
| 2                 | Ag                     | cyclohexanol | Air                                     | 340              | 53                          | 51                      | [10]      |
| 3                 | Ag/ZFC                 | cyclohexanol | O <sub>2</sub> :N <sub>2</sub> (1:15)   | 320              | 38                          | 23                      | [11]      |
| 4                 | Mn/MCM-41              | cyclohexanol | Air                                     | 250              | 52                          | 39                      | [12]      |
| 5                 | CoO/Ag                 | cyclohexanol | O <sub>2</sub> :N <sub>2</sub> (1:7.45) | 280              | 79                          | 75                      | [13]      |
| 6                 | Au/SiO <sub>2</sub>    | cyclohexanol | O <sub>2</sub>                          | 230              | 35.7                        | 35.7                    | [14]      |
| 7                 | AuNi/SiO <sub>2</sub>  | cyclohexanol | O <sub>2</sub>                          | 240              | 10.2                        | 10.2                    | [15]      |
| 8                 | Pt/CuClP               | KA-oil       | Air                                     | 200              | 74                          | 74                      | [5]       |
| 9 <sup>[b]</sup>  | Au/SiO <sub>2</sub>    | KA-oil       | O <sub>2</sub>                          | 230              | 11.4                        | 11.4                    | This work |
| 10 <sup>[c]</sup> | Pt/SiO <sub>2</sub> -O | KA-oil       | Air                                     | 170              | 85.4                        | 78.1                    | This work |
| 11 <sup>[c]</sup> | Pt/SiO <sub>2</sub> -H | KA-oil       | Air                                     | 170              | 45.3                        | 37.4                    | This work |

[a] KA-oil consists of 1:1 weight ratio of cyclohexanone and cyclohexanol. [b] Reaction condition: 1 wt% Au loading, 0.1 g catalyst mixed with 1.2 g quartz sand, O<sub>2</sub> = 4 mL min<sup>-1</sup>, KA-oil = 0.4 mL h<sup>-1</sup>. [c] Reaction condition: 1 wt% Pt loading, 0.2 g catalyst mixed with 1.2 g quartz sand, air = 16 mL min<sup>-1</sup>, KA-oil = 0.4 mL h<sup>-1</sup>. The carbon balance is > 95%.

synthesis,<sup>[6]</sup> it is proposed recently that gas molecules adsorbed on specific crystal faces can also induce a shape evolution.<sup>[7]</sup> While environmental transmission electron microscopy (ETEM) studies and theoretical calculations have verified the feasibility of this approach,<sup>[7a,8]</sup> few studies have utilized it to rationally design practical catalysts. Considering the different adsorption behavior of O<sub>2</sub> and H<sub>2</sub> on Pt surface,<sup>[8]</sup> we reason that calcinating Pt precursors in O<sub>2</sub> and H<sub>2</sub> will produce different shaped PtNPs.

Figure 1a shows a typical TEM image of Pt/SiO<sub>2</sub>-O. Clearly, some cube-like Pt particles have formed after calcination in O<sub>2</sub> atmosphere (see Figure S1 for more TEM images). Statistical analysis suggests that Pt particles in Pt/SiO<sub>2</sub>-O consist of 51%

cubic shapes, 34% irregular shapes and only 15% spherical shapes. The high-resolution TEM (HRTEM) image (Figure 1b) of a cube-like particle of Pt/SiO<sub>2</sub>-O shows continuous lattice fringes with a lattice spacing of 0.197 nm, which corresponds to the (200) plane of Pt. The spots in the fast Fourier transform (FFT) pattern also confirm that PtNPs in Pt/SiO<sub>2</sub>-O are single-crystal Pt nanocubes (Figure 1b inset).<sup>[9]</sup> In contrast, more round-edged PtNPs are observed in Pt/SiO<sub>2</sub>-H sample (Figure 1c and Figure S2). Pt particles in Pt/SiO<sub>2</sub>-H consist of 83% spherical shapes, 12% irregular shapes and only 5% cubic shapes. The lattice fringes of a spherical Pt particle show an interplanar spacing of 0.224 nm, corresponding to the (111) plane of Pt (Figure 1d). The different morphology of PtNPs obtained by calcinations can be well explained by the previous reported theoretical calculations and ETEM studies. Yuan *et al.* proposed that low coordinated Pt(100) surface binds O<sub>2</sub> more strongly compared to the closely packed Pt(111) surface.<sup>[8a]</sup> The stronger adsorption of O<sub>2</sub> might therefore lead to the extension of (100) faces and the shrink of (111) faces.<sup>[7a]</sup> On the other hand, H<sub>2</sub> prefers to adsorb on Pt(111) surface,<sup>[8b]</sup> which might consequently produce rounded shapes or truncated octahedral shapes.<sup>[7a]</sup>

Unlike the different morphology, Pt/SiO<sub>2</sub> samples calcined at different atmospheres show similar XRD patterns (Figure S3). The characteristic diffraction peaks at  $2\theta = 39.8$ ,  $46.3$  and  $67.5^\circ$  can be readily assigned to (111), (200), and (220) of Pt (PDF#04-0802). The average Pt particle size of Pt/SiO<sub>2</sub>-O (21.5 nm) is close to that of Pt/SiO<sub>2</sub>-H (17.8 nm), indicating that the different calcination atmospheres won't significantly change the average particle size. CO pulse chemisorption results indicate that the Pt dispersions of Pt/SiO<sub>2</sub>-O and Pt/SiO<sub>2</sub>-H are similar (3.52% vs. 3.71%, Table 2). X-ray photoelectron spectroscopy (XPS) analysis shows no visible signals of chlorine (Figure S4), suggesting that H<sub>2</sub>PtCl<sub>6</sub> is completely decomposed into PtNPs. Besides, Pt 4f XPS data (Figure S5) also confirm that Pt<sup>0</sup> is the major phase in both samples. A small amount of Pt<sup>4+</sup> species is detected in fresh Pt/SiO<sub>2</sub>-O, likely due to the formation of PtO<sub>2</sub> on the surface of PtNPs. This species can be easily reduced by cyclohexanol and therefore disappears in the spent catalyst. Taking all together, Pt/SiO<sub>2</sub>-O and Pt/SiO<sub>2</sub>-H provide excellent

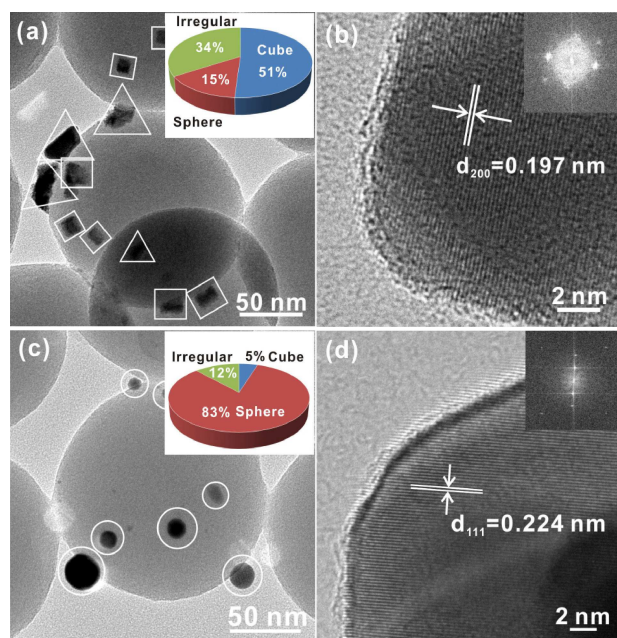


**Figure 1.** TEM images of Pt/SiO<sub>2</sub>-O (a) and Pt/SiO<sub>2</sub>-H (c). The insets show the statistic distribution of different shaped Pt NPs. HRTEM images of Pt particles of Pt/SiO<sub>2</sub>-O (b) and Pt/SiO<sub>2</sub>-H (d). The insets show FFT patterns of the lattice images in (b) and (d). The squares, circles and triangles in the figures represent the cubic, spherical and irregular shapes, respectively.

| Catalyst               | Pt surface area [m <sup>2</sup> g <sub>cat</sub> <sup>-1</sup> ] <sup>[a]</sup> | Dispersion (D) [%] <sup>[a]</sup> | Particle size, d [nm] Chemisorption <sup>[b]</sup> | XRD <sup>[c]</sup> |
|------------------------|---|-----------------------------------|--|--------------------|
| Pt/SiO <sub>2</sub> -O | 0.087   | 3.52                              | 32.1   | 21.5               |
| Pt/SiO <sub>2</sub> -H | 0.092   | 3.71                              | 30.4   | 17.8               |

[a] Estimated from CO pulse chemisorption; [b] Based on  $d$  (nm) = 1.13/D.<sup>[16]</sup>  
[c] Based on the Scherrer equation.

models to investigate the morphology effect on their catalytic performances.

Figure 2a shows the catalytic activity and selectivity of Pt/SiO<sub>2</sub>-O and Pt/SiO<sub>2</sub>-H in ODH of KA-oil. In all cases, the main by-product is CO<sub>2</sub>. Other by-products are benzene, cyclohexene and 2-cyclohexen-1-one and the selectivities of these compounds are all less than 0.1%. Notably, Pt/SiO<sub>2</sub>-O shows very good cyclohexanol conversion and cyclohexanone selectivity at full temperature ranges (165–185 °C). The cyclohexanone yield of Pt/SiO<sub>2</sub>-O reaches 78.1% even at a temperature as low as 170 °C, surpassing most of the literature results (Table 1). It is important to highlight that at 165 °C, the cyclohexanone yield of Pt/SiO<sub>2</sub>-O is about 3 times larger than that of Pt/SiO<sub>2</sub>-H (74.3% vs. 24.2%), which clearly indicates the great influence of the calcination atmosphere. The different morphology of PtNPs induced by the calcination atmosphere might account for this

significant catalytic difference. Besides, as the temperature increases from 165 to 180 °C, the cyclohexanol conversion of Pt/SiO<sub>2</sub>-H increases from 29.8% to 64.3%. Further increasing the temperature to 185 °C, however, slightly decreases the conversion of cyclohexanol, likely due to the competitive adsorption between cyclohexanol and cyclohexanone. The cyclohexanone selectivity of Pt/SiO<sub>2</sub>-O is always about 10% higher than that of Pt/SiO<sub>2</sub>-H in the temperature range of 165–185 °C, supporting an inference that Pt/SiO<sub>2</sub>-O favors the adsorption of cyclohexanol over cyclohexanone than Pt/SiO<sub>2</sub>-H.

To verify this inference, we conducted comparison studies of the reaction kinetic on Pt/SiO<sub>2</sub>-O and Pt/SiO<sub>2</sub>-H. As shown in Figure 2b, the apparent activation energies of cyclohexanol ODH reaction over Pt/SiO<sub>2</sub>-O and Pt/SiO<sub>2</sub>-H are close (61.0 vs. 56.4 kJ mol<sup>-1</sup>), implying identical reaction pathways in these two cases. Additionally, O<sub>2</sub> partial pressure experiments suggest that there is only a small change of the apparent reaction order of O<sub>2</sub> molecules on Pt/SiO<sub>2</sub>-O and Pt/SiO<sub>2</sub>-H (0.82 vs. 0.77, Figure 2c). However, the apparent reaction order of cyclohexanol on Pt/SiO<sub>2</sub>-O is 0.13 (Figure 2d), obviously smaller than that on Pt/SiO<sub>2</sub>-H (0.36). Based on the classic theory, smaller reaction order indicates stronger adsorption on the surface of catalyst.<sup>[17]</sup> Therefore, we come to the conclusion that O<sub>2</sub> adsorption is not the decisive factor for the activity difference, whereas cyclohexanol adsorption is the key point.

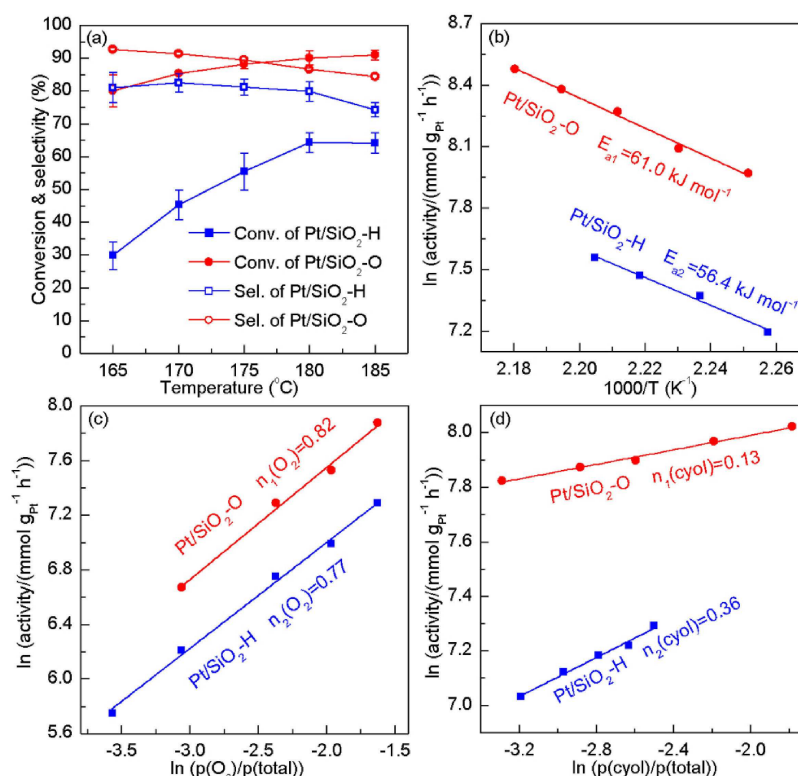


**Figure 2.** (a) Cyclohexanol conversion and cyclohexanone selectivity of Pt/SiO<sub>2</sub>-O and Pt/SiO<sub>2</sub>-H in ODH of KA-oil. Reaction condition: 0.2 g catalyst mixed with 1.2 g quartz sand, air = 16 mL min<sup>-1</sup>, KA-oil = 0.4 mL h<sup>-1</sup>. The carbon balance is > 95%. (b) The Arrhenius plots of Pt/SiO<sub>2</sub>-O and Pt/SiO<sub>2</sub>-H in ODH of cyclohexanol. The influence of O<sub>2</sub> (c) and cyclohexanol (d) partial pressure on catalytic activity of Pt/SiO<sub>2</sub>-O and Pt/SiO<sub>2</sub>-H in ODH of cyclohexanol. The activity is calculated based on the mole number of converted cyclohexanol molecules. Cyol represents cyclohexanol.

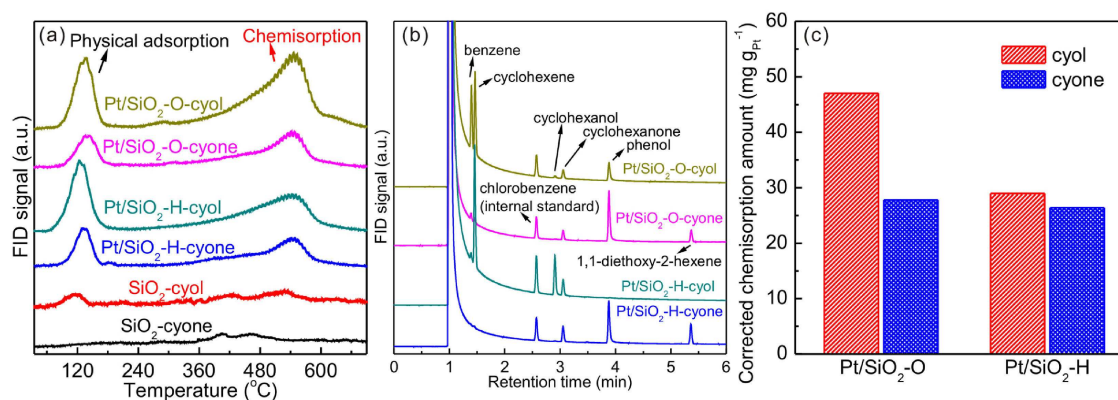


**Figure 3.** (a) TPD curves of cyclohexanol and cyclohexanone on SiO<sub>2</sub> support, Pt/SiO<sub>2</sub>-O and Pt/SiO<sub>2</sub>-H. (b) FID peaks of collected species desorbed in the high-temperature region of TPD experiments. (c) The corrected amount of chemisorbed cyclohexanol and cyclohexanone on Pt/SiO<sub>2</sub>-O and Pt/SiO<sub>2</sub>-H. Cyol and cyone represent cyclohexanol and cyclohexanone, respectively.

Temperature-programmed desorption (TPD) measurements were then carried out to quantify the amount of chemisorbed cyclohexanol and cyclohexanone on Pt/SiO<sub>2</sub>-O and Pt/SiO<sub>2</sub>-H. As shown in Figure 3a, TPD curves of cyclohexanol- or cyclohexanone-adsorbed Pt/SiO<sub>2</sub> catalysts show two distinct signals. The one located at low-temperature region belongs to the physical adsorption and the other located at high-temperature region is assigned to the chemisorbed molecules which have stronger interaction with Pt/SiO<sub>2</sub> catalysts. Control experiments show that SiO<sub>2</sub> support seldom chemisorbs cyclohexanol or cyclohexanone. Thus, the chemisorbed molecules are contributed by PtNPs. To further understand the TPD data, we collected the desorbed species in the high-temperature region and analyzed them with GC-FID and GC-MS. As shown in Figure 3b, benzene, cyclohexene, phenol and 1,1-diethoxy-2-hexene (possibly deriving from 2-hexenal and ethanol) in addition to cyclohexanol and cyclohexanone are detected, indicating that the chemisorbed cyclohexanol and cyclohexanone are decomposed on Pt surfaces at high temperatures before desorbed into gas phase. Thus, in this situation, the desorption temperature cannot stand for the adsorption strength. By adding together the amount of all products, we could infer the initial adsorption amount of cyclohexanol or cyclohexanone. As shown in Figure 3c, the initial adsorption amount of cyclohexanol on Pt/SiO<sub>2</sub>-O (47.0 mg g<sub>Pt</sub><sup>-1</sup>) is obviously larger than that on Pt/SiO<sub>2</sub>-H (29.0 mg g<sub>Pt</sub><sup>-1</sup>), in good agreement with their activity difference. Moreover, on Pt/SiO<sub>2</sub>-O, the initial adsorption amount of cyclohexanol is 1.69 times as large as that of cyclohexanone (27.8 mg g<sub>Pt</sub><sup>-1</sup>), which further explains its excellent catalytic performance in ODH of KA-oil.

To further prove that the catalytic difference between Pt/SiO<sub>2</sub>-O and Pt/SiO<sub>2</sub>-H is caused by the different morphology, PtNPs with specific shapes were synthesized using reported methods.<sup>[18]</sup> As shown in Figure 4a, the synthesized cubic PtNPs have an average size of 15.3 ± 1.7 nm (diagonal), containing about 68% cubes (consisting of only Pt(100)). On the other hand, the synthesized octahedral PtNPs have an average size of

15.1 ± 2.5 nm (longer diagonal, Figure 4d), containing about 74% octahedrons (consisting of only Pt(111)). HRTEM images in Figure 4b and 4e show the lattice spacing of 0.199 nm and 0.230 nm, corresponding to the typical (200) and (111) plane of Pt cubes and octahedrons, respectively. The synthesized cubic and octahedral nanoparticles were loaded onto SiO<sub>2</sub> by a colloid deposition method, followed by a thermal treatment at 250 °C. As shown in Figure 4c and 4f, the PtNPs basically maintain the sizes and the desired shapes. XRD patterns (Figure S6) indicate that there is no detectable KCl or NaCl residual from synthesis processes in these two catalysts.

The catalytic activity and selectivity of Pt cubes/SiO<sub>2</sub> and Pt octahedrons/SiO<sub>2</sub> in ODH of KA-oil are shown in Figure 5a. The cyclohexanone selectivity of cubes is close to that of octahedrons, whereas the cyclohexanol conversion of cubes is higher than that of octahedrons by about 25–35% in the temperature range of 165–185 °C, in good agreement with the catalytic performances of Pt/SiO<sub>2</sub>-O and Pt/SiO<sub>2</sub>-H. Moreover, the apparent reaction order of cyclohexanol on Pt cubes/SiO<sub>2</sub> is smaller than that on Pt octahedrons/SiO<sub>2</sub> as expected (0.26 vs. 0.41, Figure 5b), suggesting stronger cyclohexanol adsorption ability of cubes. A similar situation is observed in the apparent reaction order of O<sub>2</sub> molecules on cubes and octahedrons (0.59 vs. 0.79, Figure 5c). Furthermore, TPD measurements (Figure S7 and 5d) suggest the initial adsorption amount of cyclohexanol on cubes (40.1 mg g<sub>Pt</sub><sup>-1</sup>) is not only larger than that on octahedrons (28.0 mg g<sub>Pt</sub><sup>-1</sup>) but also larger than the initial adsorption amount of cyclohexanone on cubes (26.5 mg g<sub>Pt</sub><sup>-1</sup>). This result provides another convincing evidence that cyclohexanol can be adsorbed on cubic Pt particles more easily, which leads to a better catalytic performance in ODH of KA-oil.

To rationalize the experimental observations, we further performed density functional theory (DFT) calculations to determine the adsorption properties of cyclohexanol and cyclohexanone at PtNPs. The cubic and octahedral PtNPs were modelled by Pt(100) and Pt(111) facets, respectively. As shown in Figure 6, the adsorption energy of the most stable binding configuration for cyclohexanol on Pt(100) is obviously higher

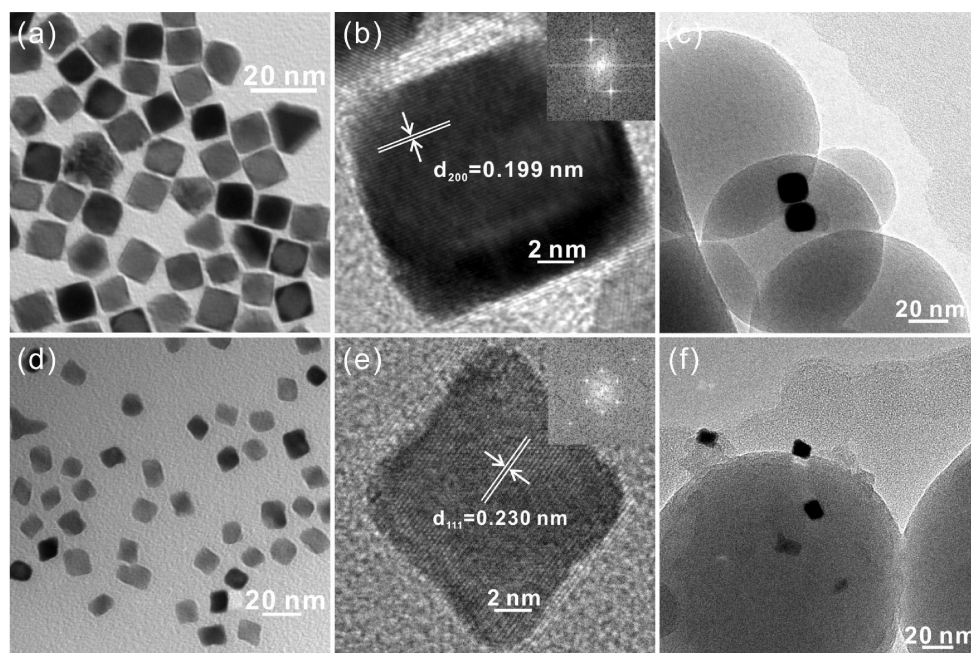


**Figure 4.** TEM images of cubic particles (a), cubes/SiO<sub>2</sub> after calcination (c), octahedral particles (d) and octahedrons/SiO<sub>2</sub> after calcination (f). HRTEM images of a cube (b) and an octahedron (e). The insets show FFT patterns of the lattice images in (b) and (e).

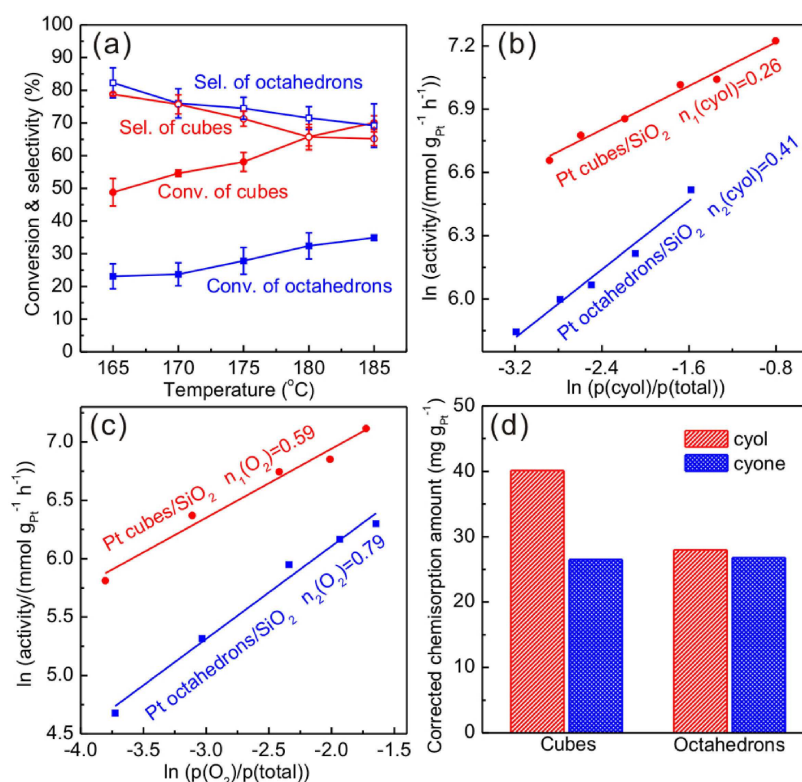


**Figure 5.** (a) Cyclohexanol conversion and cyclohexanone selectivity of Pt cubes/SiO<sub>2</sub> and Pt octahedrons/SiO<sub>2</sub> in ODH of KA-oil. Reaction condition: 0.2 g catalyst mixed with 1.2 g quartz sand, air = 16 mL min<sup>-1</sup>, KA-oil = 0.4 mL h<sup>-1</sup>. The main byproduct is CO<sub>2</sub> and the carbon balance is > 95%. The influence of cyclohexanol (b) and O<sub>2</sub> (c) partial pressure on catalytic activity in ODH of cyclohexanol. The activity is calculated based on the mole number of converted cyclohexanol molecules. (d) The amount of chemisorbed cyclohexanol and cyclohexanone on Pt cubes/SiO<sub>2</sub> and Pt octahedrons/SiO<sub>2</sub>.

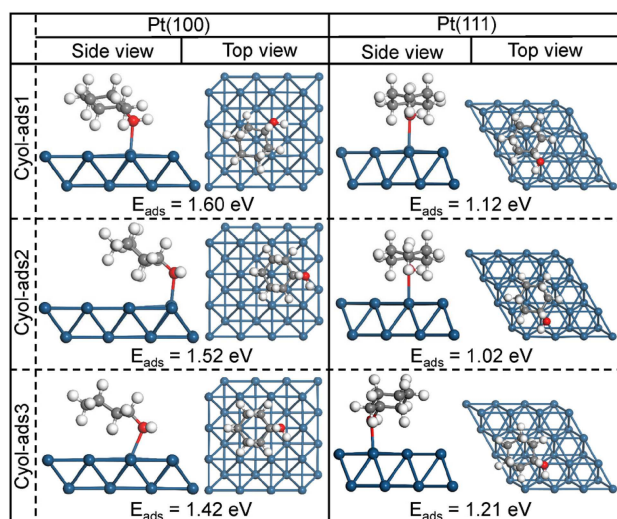


**Figure 6.** Calculated binding configurations and corresponding adsorption energies of the cyclohexanol at Pt(100) and Pt(111). Pt atoms are in blue, C in gray, O in red and H in white. Cyol represents cyclohexanol.

than that on Pt(111) (1.60 eV vs. 1.21 eV). This result clearly indicates stronger chemisorption of cyclohexanol on Pt(100)

than on Pt(111), being consistent with the result obtained from partial pressure experiments. Besides, the adsorption energies of the most stable binding configurations for cyclohexanone (Figure S8) on both Pt(100) and Pt(111) are smaller than those for cyclohexanol, which is consistent with the relative good selectivity of cyclohexanone on Pt cubes/SiO<sub>2</sub> and Pt octahedrons/SiO<sub>2</sub> (Figure 5a).

Taking all these results together, both the experimental data and theoretical calculations show that cubic PtNPs possess stronger adsorption ability to cyclohexanol than octahedral PtNPs and therefore display better catalytic activity in ODH of KA-oil. In the case of Pt/SiO<sub>2</sub>-O, many cube-like particles have formed after calcination in O<sub>2</sub> atmosphere and these particles help to improve the catalytic performance as a consequence.

Moreover, the catalytic stability of Pt/SiO<sub>2</sub>-O catalyst was investigated under the applied reaction condition. As shown in Figure 7a, the cyclohexanone selectivity is maintained at about 88% all the time, whereas the cyclohexanol conversion decreases from 87.6% to 72.1% (17.7% activity loss) after a 100-hour test. XRD analysis in Figure 7b shows that the average particle size of PtNPs after reaction is nearly the same as that of fresh catalyst. Figure 7c displays a TEM image of spent Pt/SiO<sub>2</sub>-O catalyst. As we can see, the cube-like PtNPs formed by calcination in O<sub>2</sub> atmosphere are quite stable during low-temperature gas-phase ODH reaction. Thus, the deactivation is

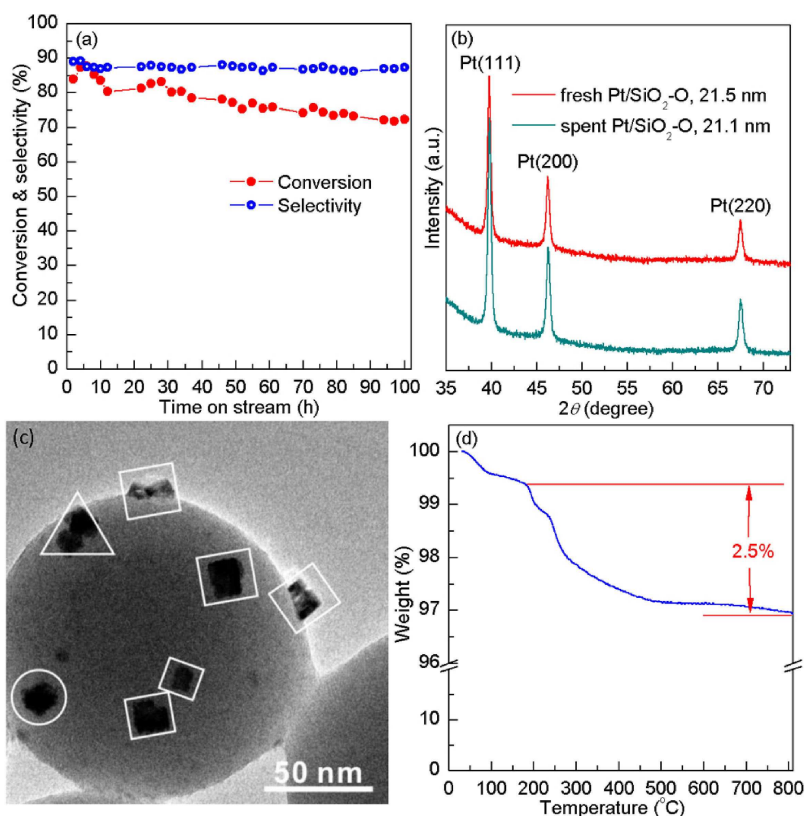


**Figure 7.** (a) Long-term stability test of Pt/SiO<sub>2</sub>-O catalyst. Reaction condition: 0.2 g catalyst mixed with 1.2 g quartz sand, temperature = 175 °C, air = 16 mL min<sup>-1</sup>, KA-oil = 0.4 mL h<sup>-1</sup>. (b) XRD patterns of fresh and spent Pt/SiO<sub>2</sub>-O catalyst. (c) TEM image of spent Pt/SiO<sub>2</sub>-O catalyst. The squares, circles and triangles in the figure represent the cubic, spherical and irregular shapes, respectively. (d) TGA curve of spent Pt/SiO<sub>2</sub>-O catalyst. Test condition: O<sub>2</sub> flow = 50 mL min<sup>-1</sup>, heating rate = 10 °C min<sup>-1</sup>.

not likely caused by the change of size or morphology. Further thermogravimetric analysis (TGA) in Figure 7d indicates that there are 2.5 wt% carbon species formed, which are believed to result in a mild deactivation. Strategies that can further improve the yield of cyclohexanone and the catalytic stability merit further study beyond the scope of this paper.

## Conclusions

In summary, we have successfully regulated the morphology of PtNPs by tuning the calcination atmosphere and applied them in gas-phase ODH of KA-oil. The strong interaction between O<sub>2</sub> and Pt(100) plane ensures the production of cube-like PtNPs by calcinating Pt/SiO<sub>2</sub> in O<sub>2</sub> atmosphere. The cyclohexanone yield of Pt/SiO<sub>2</sub>-O catalyst can reach up to 78.1% at a relatively low temperature of 170 °C, surpassing most of the reported results. Experimental and theoretical calculation results reveal that these cube-like PtNPs help to strengthen the adsorption of cyclohexanol, which is vitally important to the outstanding catalytic performance in ODH of KA-oil. Though the current catalytic system is still far from achieving a 100% cyclohexanone yield to omit extra alcohol-ketone separation process, it takes a valuable step forward. It is expected that the outcome of this work will help to accelerate the design of more efficient and durable catalysts not only for gas-phase ODH of KA-oil but also for other structure-sensitive reactions.<sup>[4b,e,19]</sup>

## Experimental Section

### Materials and Reagents

H<sub>2</sub>PtCl<sub>6</sub>·6H<sub>2</sub>O (AR), NaNO<sub>3</sub> (AR), NaBH<sub>4</sub> (98%), tetraethyl orthosilicate (TEOS, AR), ethylene glycol (EG, AR), cyclohexanone (AR) and ammonium hydroxide aqueous solution (25%) were purchased from Sinopharm Chemical Reagent Co., Ltd. Poly(vinylpyrrolidone) (PVP, *M<sub>w</sub>* = 58 000) and tetradecyltrimethylammonium bromide (TTAB, 99%) were purchased from Aladdin. K<sub>2</sub>PtCl<sub>4</sub> (99.9%) was purchased from Alfa Aesar. Cyclohexanol (AR, ≥98.5%) was obtained from Macklin. KA-oil consisted of 1:1 weight ratio of cyclohexanone (AR) and cyclohexanol (AR, ≥98.5%). All chemicals were used without further purification.

### Catalysts preparation

**Synthesis of silica nanospheres.** Silica nanospheres were synthesized using a classic Stöber method.<sup>[20]</sup> Typically, 18 mL of ammonium hydroxide aqueous solution (25%) and 6 mL of deionized water were mixed with 360 mL of ethanol, followed by vigorous stirring for 0.5 h at 25 °C. Subsequently, 13.8 mL of TEOS was added to this solution. The mixture was stirred vigorously for 6 h and was then centrifuged, washed with ethanol and dried at 65 °C. The obtained silica nanospheres were calcined at 600 °C in dry air for 5 h to remove residual organic groups and most of surface hydroxyl groups before use.

**Preparation of 1 wt% Pt/SiO<sub>2</sub>.** 3.32 mL of 7.72 mM H<sub>2</sub>PtCl<sub>6</sub>·6H<sub>2</sub>O ethanol solution was mixed with 0.5 g of silica nanospheres at room temperature. The mixture was evaporated slowly with vigorous stirring and was then transferred into a 65 °C oven for 3 h.

Finally, the pale-yellow powder was calcined in H<sub>2</sub> or O<sub>2</sub> for 5 h, denoted as Pt/SiO<sub>2</sub>-H and Pt/SiO<sub>2</sub>-O, respectively. Due to the high thermal decomposition temperature of PtCl<sub>2</sub> (570 °C under non-reductive atmosphere),<sup>[21]</sup> the calcination temperature was set to 600 °C.

**Synthesis of Pt cubes.** The synthesis of Pt cubes was performed using TTAB as a protector and NaBH<sub>4</sub> as a reductant.<sup>[4e,18a]</sup> A solution containing 9.3 mL of deionized water, 7.5 mL of 0.4 M TTAB aqueous solution and 2.0 mL of 15.0 mM K<sub>2</sub>PtCl<sub>4</sub> aqueous solution was introduced in a 50 mL vial. The vial reactor was kept at 50 °C with magnetic stirring. After the solution became clear, 1.2 mL of a fresh 0.75 M NaBH<sub>4</sub> aqueous solution was added. The vial reactor kept connected to the open air for 10 min and was then sealed for 6 h. The product was centrifuged at 3 krpm for 30 min. The supernatant solution was further centrifuged at 14 krpm for 10 min. The black precipitate was redispersed in deionized water and the solution was centrifuged at 14 krpm for 10 min. Finally, the precipitate was collected and redispersed in deionized water.

**Synthesis of Pt octahedrons.** The Pt octahedrons were synthesized by the reduction of H<sub>2</sub>PtCl<sub>6</sub> by EG in the presence of PVP and NaNO<sub>3</sub> under air.<sup>[18b]</sup> Briefly, 1 mL of 80 mM H<sub>2</sub>PtCl<sub>6</sub> solution in EG was rapidly added to 7 mL EG (kept at 160 °C) which contained both PVP and NaNO<sub>3</sub>. The final solution consisted of 10 mM H<sub>2</sub>PtCl<sub>6</sub>, 30 mM PVP and 55 mM NaNO<sub>3</sub>. After reacting for 20 min, the product was precipitated by adding 24 mL of acetone and was then washed twice by a mixed solvent consisting of 5 mL of ethanol and 15 mL of *n*-hexane. Finally, the product was redispersed in ethanol using sonication.

**Preparation of 1 wt% Pt cubes/SiO<sub>2</sub> and 1 wt% Pt octahedrons/SiO<sub>2</sub>.** 0.5 g of silica nanospheres were added to Pt colloidal solution containing 5 mg Pt (verified by inductively coupled plasma-atomic emission spectrometry). The mixture was stirred vigorously at room temperature until the solvent was evaporated to dryness and was then transferred into a 65 °C oven for 3 h. In order to minimize the contamination on the surface of Pt particles and preserve the desired particle shape simultaneously, the grey powder was calcined at 250 °C in O<sub>2</sub> for 1 h and then in H<sub>2</sub> for another 1 h.<sup>[4b]</sup> The oxidation-reduction cycle was repeated twice.

### Characterization

Transmission electron microscopy (TEM) images were recorded on the Hitachi HT-7700 microscope operated at 100 kV. High-resolution TEM images were recorded on the FEI Tecnai G2 F20 S-TWIN microscope operated at 200 kV. Wide-angle X-ray diffraction (XRD) patterns were recorded on a Rigaku Ultimate IV diffractometer using Cu K<sub>α</sub> radiation. The average particle size was derived from the Scherrer equation based on the peak width of the Pt(111) reflection. Thermogravimetric analysis (TGA) curve was recorded with STA409PC TG-DTA/DSC analyzer. The temperature-programmed desorption (TPD) curves were recorded using GC-FID. N<sub>2</sub> was used as carrier gas and was controlled at 100 mL min<sup>-1</sup>. The prepared Pt/SiO<sub>2</sub> catalysts were pretreated by cyclohexanol or cyclohexanone supplied through a syringe pump at a speed of 0.6 mL h<sup>-1</sup> at 165 °C for 1 h. Then, N<sub>2</sub> continued to sweep at 100 mL min<sup>-1</sup> for 2 h to remove the weakly adsorbed species. Subsequently, 10 mg of the pretreated sample was placed in a quartz tube fixed by silica wool. The sample was swept by N<sub>2</sub> at room temperature at a speed of 200 mL min<sup>-1</sup>. The sweeping N<sub>2</sub> flow was then introduced into GC-FID. After the baseline of GC-FID became stable, the TPD was carried out from 25 to 690 °C with a heating rate of 5 °C min<sup>-1</sup>. For the offline collection experiment, 2.5 g of the pretreated sample (40–100 mesh) and a cold trap filled with ethanol were used. The collection started from 290 °C to

520 °C and held at 520 °C for 1 h. Chlorobenzene was used as the internal standard for quantitative analysis of the desorbed species.

### Catalytic Reaction

The gas-phase oxidative dehydrogenation (ODH) of KA-oil was performed within an electronically controlled furnace in a fixed bed vertical glass reactor (length = 250 mm, inner diameter = 12 mm), fitted with a glass frit carrying the catalyst mixed with quartz sand. Standard air (21% O<sub>2</sub> and 79% N<sub>2</sub>) was used as oxidant. The air stream (16 mL min<sup>-1</sup>) was controlled by a mass flow instrument and the liquid reagent (0.4 mL h<sup>-1</sup>) was supplied through a syringe pump. Liquid vaporization occurred on the reactor wall prior to the catalytic bed. The reaction ran for 1.5 h to reach equilibrium before every sampling. Afterwards, liquid- and gas-phase products were collected at the same time. Liquid-phase products were analyzed by GC-FID equipped with a 30 m SE-54 column using 2 M triethylene glycol dimethyl ether in acetone as internal standard. Gas-phase products were analyzed by GC-TCD equipped with a 1 m TDX-01 column and CO<sub>2</sub> was the only gas-phase product. Conversion and selectivity were calculated combining both liquid- and gas-phase analytic results.

### Partial Pressure Experiments

The catalytic bed temperature was kept at 170 °C during partial pressure experiments. The charging rate of gas stream and cyclohexanol were controlled by a mass flow instrument and a syringe pump, respectively. For the control of O<sub>2</sub> partial pressure, N<sub>2</sub> was used as balance gas and total flow rate was kept at 16 mL min<sup>-1</sup>, of which the air flow rate (0 to 16 mL min<sup>-1</sup>) was adjusted to certain ratios with cyclohexanol (0.4 mL h<sup>-1</sup>). For the control of cyclohexanol partial pressure, air flow rate was fixed at 16 mL min<sup>-1</sup> while the charging rate of cyclohexanol was adjusted (0 to 1.2 mL h<sup>-1</sup>). Product analysis was similar to the gas-phase ODH of KA-oil.

### DFT Calculations

Density functional theory (DFT) calculations were carried out using the Vienna Ab-initio Simulation Package (VASP).<sup>[22]</sup> The spin-polarized projector augmented wave (PAW) method<sup>[23]</sup> and the Perdew–Burke–Ernzerhof (PBE)<sup>[24]</sup> electron exchange–correlation functional of the generalized gradient approximation (GGA)<sup>[25]</sup> were applied in our calculations. The kinetic energy cut-off for the wave function expanded in the plane-wave basis was set as 400 eV. To optimize the structures, the calculation was performed until the maximum force upon each relaxed atom was less than 0.05 eV Å<sup>-1</sup>. The vacuum height was set as 15 Å to eliminate the interaction between neighboring slabs.

The adsorption energy ( $E_{\text{ads}}$ ) was calculated as follows [Eq. (1)]:

$$E_{\text{ads}} = -(E_{\text{total}} - E_{\text{substrate}} - E_{\text{gas-phase adsorbate}}) \quad (1)$$

where  $E_{\text{total}}$  is the calculated total energy of the adsorption system,  $E_{\text{substrate}}$  is the energy of the clean substrate and  $E_{\text{gas-phase adsorbate}}$  is the energy of the gas-phase molecule.

To study the adsorption of cyclohexanol and cyclohexanone on Pt (111) and Pt(100) surfaces, we used the following models: a 4×4 surface cell was used to construct a six-layer Pt(111) and Pt(100) slab, the top three layers of the Pt(111) and Pt(100) slab were allowed to relax. The Brillouin-zone integration was performed

along with a 2×2×1 Monkhorst-Pack grid for the different surface slabs.

### Acknowledgements

This work was supported by National Natural Science Foundation of China (91545113, 91545103, 21573067), China Postdoctoral Science Foundation (512200-X91701), Shell Global Solutions International B. V. (PT71423, PT74557), Fok Ying Tong Education Foundation (131015) and the Fundamental Research Funds for the Central Universities (2014XZZX003-02).

### Conflict of Interest

The authors declare no conflict of interest.

**Keywords:** Pt/SiO<sub>2</sub> · Calcination atmosphere · Morphology · Oxidative dehydrogenation · KA-oil

- [1] a) B. M. Nagaraja, V. Siva Kumar, V. Shashikala, A. H. Padmasri, S. Sreevardhan Reddy, B. David Raju, K. S. Rama Rao, *J. Mol. Catal. A* **2004**, *223*, 339–345; b) S. A. Chavan, D. Srinivas, P. Ratnasamy, *J. Catal.* **2002**, *212*, 39–45; c) A. Valente, Z. Lin, P. Brandão, I. Portugal, M. Anderson, J. Rocha, *J. Catal.* **2001**, *200*, 99–105; d) H. Liu, T. Jiang, B. Han, S. Liang, Y. Zhou, *Science* **2009**, *326*, 1250–1252.
- [2] a) X. Fang, Z. Yin, H. Wang, J. Li, X. Liang, J. Kang, B. He, *J. Catal.* **2015**, *329*, 187–194; b) A. A. Alshaheri, M. I. M. Tahir, M. B. A. Rahman, T. B. S. A. Ravoof, T. A. Saleh, *Chem. Eng. J.* **2017**, *327*, 423–430; c) R. Raja, G. Sankar, J. M. Thomas, *J. Am. Chem. Soc.* **1999**, *121*, 11926–11927; d) Y. Liu, H. Tsunoyama, T. Akita, S. Xie, T. Tsukuda, *ACS Catal.* **2011**, *1*, 2–6; e) Z. Xiao, W. Zhan, Y. Guo, Y. Guo, X. Gong, G. Lu, *Chin. J. Catal.* **2016**, *37*, 273–280.
- [3] a) K. Tan, K. Fujii, M. Nakamura, K. Hanada (Mitsubishi Kasei Corporation), US 5168983, **1992**; b) C. L. Becker, J. D. Davis, J. M. Dakka, K. C. Nadler (ExxonMobil Chemical Patents Inc.), US 9868687 B2, **2018**.
- [4] a) Y. Zhou, Y. Zhu, Z. Q. Wang, G. Ma, M. Xia, X. Kong, L. Xiao, X. Q. Gong, J. Fan, *J. Am. Chem. Soc.* **2017**, *139*, 13740–13748; b) I. Lee, R. Morales, M. A. Albiter, F. Zaera, *Proc. Natl. Acad. Sci. USA* **2008**, *105*, 15241–15246; c) I. Lee, F. Delbecq, R. Morales, M. A. Albiter, F. Zaera, *Nat. Mater.* **2009**, *8*, 132–138; d) M. Englisch, A. Jentys, J. A. Lercher, *J. Catal.* **1997**, *166*, 25–35; e) K. M. Bratlie, H. Lee, K. Komvopoulos, P. Yang, G. A. Somorjai, *Nano Lett.* **2007**, *7*, 3097–3101.
- [5] A. M. Gill, C. S. Hinde, R. K. Leary, M. E. Potter, A. Jouve, P. P. Wells, P. A. Midgley, J. M. Thomas, R. Raja, *ChemSusChem* **2016**, *9*, 423–427.
- [6] a) T. S. Ahmadi, Z. L. Wang, T. C. Green, A. Henglein, M. A. El-Sayed, *Science* **1996**, *272*, 1924–1925; b) A. R. Tao, S. Habas, P. Yang, *Small* **2008**, *4*, 310–325; c) J. Chen, B. Lim, E. P. Lee, Y. Xia, *Nano Today* **2009**, *4*, 81–95; d) Z. Peng, H. Yang, *Nano Today* **2009**, *4*, 143–164.
- [7] a) M. Cabié, S. Giorgio, C. R. Henry, M. R. Axet, K. Philippot, B. Chaudret, *J. Phys. Chem. C* **2010**, *114*, 2160–2163; b) A. S. Ramachandran, S. L. Anderson, A. K. Datye, *Ultramicroscopy* **1993**, *51*, 282–297; c) G. Rupprechter, H.-J. Freund, *Top. Catal.* **2000**, *14*, 3–14; d) M. McLean, H. Mykura, *Surf. Sci.* **1966**, *5*, 466–481; e) F. Mittendorfer, N. Seriani, O. Dubay, G. Kresse, *Phys. Rev. B* **2007**, *76*, 233413; f) H. Graoui, S. Giorgio, C. R. Henry, *Surf. Sci.* **1998**, *417*, 350–360; g) S. Giorgio, S. Sao Joao, S. Nitsche, D. Chaudanson, G. Sitja, C. R. Henry, *Ultramicroscopy* **2006**, *106*, 503–507.
- [8] a) W. Yuan, Y. Jiang, Y. Wang, S. Kattel, Z. Zhang, L.-Y. Chou, C.-K. Tsung, X. Wei, J. Li, X. Zhang, G. Wang, S. X. Mao, Z. Zhang, *Chem. Commun.* **2015**, *51*, 350–353; b) Z.-F. Gao, H. Chen, S.-T. Qi, C.-H. Yi, B.-L. Yang, *Acta Phys.-Chim. Sin.* **2013**, *29*, 1900–1906.
- [9] Y.-W. Lee, S.-B. Han, D.-Y. Kim, K.-W. Park, *Chem. Commun.* **2011**, *47*, 6296–6298.
- [10] Z. Yang, J. Li, X. Yang, X. Xie, Y. Wu, *J. Mol. Catal. A* **2005**, *241*, 15–22.

- [11] J. Shen, W. Shan, Y. Zhang, J. Du, H. Xu, K. Fan, W. Shen, Y. Tang, *J. Catal.* **2006**, *237*, 94–101.
- [12] D. Santharaj, C. Suresh, P. Vijayan, N. Venkatathri, K. Shanthi, *React. Kinet. Mech. Catal.* **2010**, *99*, 439–446.
- [13] G. Zhao, F. Yang, Z. Chen, Q. Liu, Y. Ji, Y. Zhang, Z. Niu, J. Mao, X. Bao, P. Hu, Y. Li, *Nat. Commun.* **2017**, *8*, 14039–14046.
- [14] W. Hong, X. Yan, R. Li, J. Fan, *Chin. J. Catal.* **2017**, *38*, 545–553.
- [15] W. Yi, W. Yuan, Y. Meng, S. Zou, Y. Zhou, W. Hong, J. Che, M. Hao, B. Ye, L. Xiao, Y. Wang, H. Kobayashi, J. Fan, *ACS Appl. Mater. Interfaces* **2017**, *9*, 31853–31860.
- [16] H. Song, R. M. Rioux, J. D. Hoefelmeyer, R. Komor, K. Niesz, M. Grass, P. Yang, G. A. Somorjai, *J. Am. Chem. Soc.* **2006**, *128*, 3027–3037.
- [17] a) R. Dittmeyer, G. Emig, in *Handbook of Heterogeneous Catalysis* (Eds.: G. Ertl, H. Knözinger, F. Schüth, J. Weitkamp), Wiley-VCH, Weinheim, **2008**, pp. 1727–1784; b) Y. Moro-Oka, Y. Morikawa, A. Ozaki, *J. Catal.* **1967**, *7*, 23–32.
- [18] a) H. Lee, S. E. Habas, S. Kweskin, D. Butcher, G. A. Somorjai, P. Yang, *Angew. Chem.* **2006**, *118*, 7988–7992; *Angew. Chem. Int. Ed.* **2006**, *45*, 7824–7828; b) T. Herricks, J. Chen, Y. Xia, *Nano Lett.* **2004**, *4*, 2367–2371.
- [19] a) A. Miyazaki, I. Balint, Y. Nakano, *J. Nanopart. Res.* **2003**, *5*, 69–80; b) J. W. Yoo, D. J. Hathcock, M. A. El-Sayed, *J. Catal.* **2003**, *214*, 1–7; c) R. Narayanan, M. A. El-Sayed, *J. Phys. Chem. B* **2005**, *109*, 12663–12676; d) J. C. Serrano-Ruiz, A. López-Cudero, J. Solla-Gullón, A. Sepúlveda-Escribano, A. Aldaz, F. Rodríguez-Reinoso, *J. Catal.* **2008**, *253*, 159–166.
- [20] W. Stöber, A. Fink, E. Bohn, *J. Colloid Interface Sci.* **1968**, *26*, 62–69.
- [21] G. J. Butterworth, *Fusion Technol.* **1992**, *21*, 1994–2000.
- [22] G. Kresse, J. Furthmüller, *Phys. Rev. B* **1996**, *54*, 11169–11186.
- [23] P. E. Blöchl, *Phys. Rev. B* **1994**, *50*, 17953–17979.
- [24] J. P. Perdew, K. Burke, M. Ernzerhof, *Phys. Rev. Lett.* **1996**, *77*, 3865–3868.
- [25] M. P. Teter, M. C. Payne, D. C. Allan, *Phys. Rev. B* **1989**, *40*, 12255–12263.

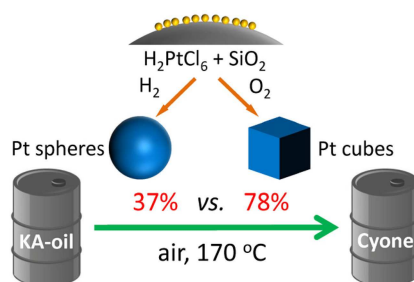
Manuscript received: August 7, 2018

Revised manuscript received: October 2, 2018

Version of record online: ■■■, ■■■■

## FULL PAPERS

**Pt does it again!** The morphology of Pt nanoparticles was successfully regulated by calcinating Pt/SiO<sub>2</sub> catalysts in different atmospheres and achieved a 78.1% cyclohexanone yield at 170 °C in oxidative dehydrogenation of KA-oil.



W. Hong, Z.-Q. Wang, Dr. S. Zou\*, Y. Zhou, Dr. L. Lu, Q. Zhou, Prof. X.-Q. Gong\*, Prof. J. Fan\*

1 – 10

**Calcination Atmosphere Regulated Morphology and Catalytic Performance of Pt/SiO<sub>2</sub> in Gas-phase Oxidative Dehydrogenation of KA-oil**

